Eur. Phys. J. Special Topics **191**, 71–89 (2010)
© EDP Sciences, Springer-Verlag 2011
DOI: 10.1140/epjst/e2010-01342-8

THE EUROPEAN PHYSICAL JOURNAL SPECIAL TOPICS

Minireview

Noninvasive optical control of complex semiconductor laser dynamics

T. Dahms[1], V. Flunkert[1], F. Henneberger[2], P. Hövel[1], S. Schikora[2], and E. Schöll[1], and H.-J. Wünsche[2]

[1] Institut für Theoretische Physik, Technische Universität Berlin, Hardenbergstraße 36, 10623 Berlin, Germany
[2] Institut für Physik, Humboldt Universität zu Berlin, Newtonstraße 15, 12489 Berlin, Germany

Received 22 November 2010 / Received in final form 23 December 2010
Published online 18 February 2011

Abstract. Time-delayed feedback control (TDFC) is transferred to the optical domain and applied to complex multisection semiconductor lasers as used in optical communication. Pyragas-type control is provided by purely optical feedback from an external Fabry-Pérot interferometer. This all-optical setup needs no time-consuming signal processing and, thus, has practically no speed limit. Proof-of-principle experiments demonstrate noninvasive stabilization of unstable steady states, chaos control, and suppression of noise-induced oscillations on picosecond time scales. A Lang-Kobayashi type model with optical TDFC is investigated taking into account the dynamic details of the device as well as all-optical time-delayed feedback. The parameter regimes that allow for stabilization of stationary emission are mapped out in good agreement with the experiments. Including noise, an analytical expression for the power spectral density is derived, which is confirmed by the experimental all-optical suppression of noise-induced relaxation oscillations.

1 Introduction

Unstable states play an important role in complex systems. They frequently interconnect attractors in phase space and thus form the skeleton of the nonlinear dynamics. Instabilities are born in various types of bifurcations. Bifurcation analysis, well-developed for ordinary and delay-differential equations, can in general uncover also the unstable objects of the phase portrait. The experimental study of unstable states, however, is difficult, because they are visited at most for short times only. Noninvasive control can overcome this difficulty: It stabilizes unstable states but does not change the states themselves, since the control forces act only if the system deviates from the state to be stabilized. Among the various methods, time-delayed feedback control (TDFC) plays an outstanding role [1], as detailed knowledge of the target state is not required here. The control force F(t) is built from the difference between the present and an earlier value of an appropriate system variable s. In the

simplest case,

$$F(t) = K[s(t-\tau) - s(t)], \tag{1}$$

with appropriate control gain $K > 0$. TDFC becomes noninvasive for orbits with period τ or steady states [2], because $s(t) = s(t-\tau)$. TDFC has been applied successfully to the stabilization of periodic orbits in a variety of systems as reviewed recently in Ref. [3].

TDFC is capable of controlling systems with fast dynamics [4], which is particularly important for semiconductor lasers. Multisection semiconductor lasers, as being used in this study, have been operated at tens of GHz [5] and the THz range is in view [6]. These picosecond time scales are too short even for fast electronic control circuits. In this context, it is desirable to perform the control entirely in the optical domain, where the speed of light sets the ultimate speed limit. All-optical control in this sense has been recently implemented experimentally and applied for the stabilization of steady states [7,8] as well as 12-GHz pulsations embedded as an unstable periodic orbit in a chaotic attractor [9]. This latter case is the fastest chaos ever controlled in a practical device. Theoretical understanding has developed accordingly [2,7,8,10–14]. The optical phase has been identified as a new parameter not present in standard theories of TDFC. Among the consequences is the possibility of circumventing the so-called odd-number limitation [15–17] treated elsewhere in this issue [18]. In the present paper, we review the noninvasive all-optical stabilization of steady states (Sec. 4) as well as periodic pulsations (Sec. 5) and present new results on the control of noise-induced oscillations (Sec. 6). These parts are preceded by tutorial introductions on the basic ingredients, i.e. multisection lasers (Sec. 2) and noninvasive optical feedback from a Fabry-Pérot interferometer (Sec. 3). The conclusion gives a summary and an outlook.

2 Dynamical regimes of multi-section semiconductor lasers

Semiconductor lasers composed of multiple longitudinal sections allow for deliberate access to numerous dynamical scenarios. Among the wide-spread applications, especially in optical communication, are mm-wave generation [19], optical clock recovery [6], signal regeneration [5], short mode-locked pulses [20], and chaos communication [21], to mention only a few. The two types of semiconductor lasers used in optical control experiments are sketched in Fig. 1(a). The devices are three-section $\lambda = 1.55\,\mu$m lasers fabricated by Fraunhofer Heinrich-Hertz-Institut Berlin. Two active sections are connected via a passive waveguide section. In the integrated tandem laser (ITL), both active sections are distributed feedback (DFB) lasers. The ITL represents the configuration of delay-coupled lasers [22]. In the amplified feedback laser (AFL), only one DFB laser is present. The other active section contains no grating and acts as a semiconductor optical amplifier. It has a cleaved facet reflecting the amplified emission of the DFB laser back to it, which provides internal optical feedback. Other facets and interfaces are nonreflecting. All sections are integrated on one semiconductor chip and are independently biased by external currents. Variation of these currents as well as temperature give rise to a four-dimensional parameter space with a rich variety of nonlinear regimes (Fig. 1(b)). Continuous wave (CW) emission represents the steady state of a laser. Its fingerprints are a single line in the optical spectrum and a noise floor in the power spectrum. Self-pulsations (SP) are T_0-periodic oscillations of the intensity. They cause a single sharp line in the power spectrum, occasionally with higher harmonics. Their optical spectrum is a comb of equidistant lines spaced by $\Delta\omega = 2\pi/T_0$. Two types of SP occur in present devices. The RO pulsations with lower frequencies are due to undamped relaxation oscillations (RO), while those in the

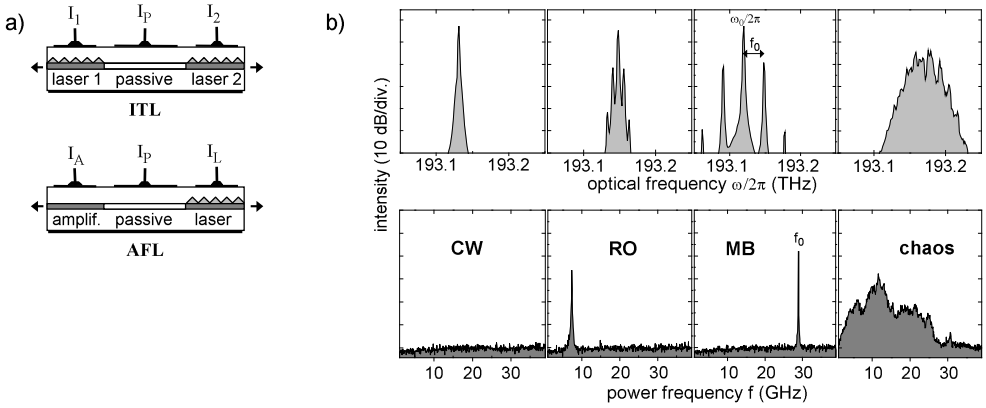

Fig. 1. Multi-section semiconductor lasers. a) The two device types used in experiments. b) Basic dynamical regimes. Upper row: optical spectra, i.e. Fourier transform of the amplitude $\mathcal{E}(t)$. Lower row: power spectra, i.e. Fourier transform of the intensity $|E(t)|^2$. From left to right: CW emission, undamped relaxation oscillations (RO), mode beating self-pulsations (MB), chaos.

few-10 GHz range denoted by MB result from mode beating (MB) between either the two detuned DFB emissions (ITL) [22] or competing optical feedback modes (AFL) [23]. Chaos is characterized by broad optical and power spectra. The transitions between the dynamical regimes take place through certain bifurcations. In the control experiments, the current I_P of the middle section is used as bifurcation parameter. It acts via the internal optical phase shift φ_P between the active sections in the laser [22–25], which should not be confused with the external phase shifts to be introduced below.

3 Noninvasive optical feedback

Optical TDFC exploits feedback from a Fabry-Pérot (FP) interferometer. Feedback from a FP has been studied previously, e.g. [26–29], but in invasive configurations, which is principally different from the noninvasive approach taken here. The experimental setup and essential parameters are schematized in Fig. 2(a). A glass etalon placed in front of the laser serves as FP. The laser output is collimated and coupled into the FP. The reflected light is reinjected in the laser and provides the control force. Noninvasive control requires that the reinjected power vanishes when the target state is reached. Thus, the optical spectrum of the target state must be a comb of equidistant lines exactly fitting the zero-reflectivity resonances of the FP as sketched in Fig. 2(b). In other words, i) the laser emits a T_0-periodic pulse sequence, ii) τ is an integer multiple of T_0, and iii) ψ is an integer multiple of 2π. Condition ii) is standard in TDFC. Resonance condition iii) is specific of optical TDFC. The necessary stability of the optical length of the FP on a subwavelength scale is achieved by using commercial glass etalons.

In the time domain, the optical field emitted by the laser is

$$\mathcal{E}(t) = \mathrm{Re}\left\{E(t)e^{i\omega_0 t}\right\}. \tag{2}$$

The exponential factor[1] represents the fast optical oscillation and the complex field $E(t)$ describes slow variations of amplitude and phase. For periodically pulsating

[1] Part of the literature uses the equivalent factor $e^{-i\omega_0 t}$, which leads to E replaced by its complex conjugate E^* in all subsequent equations.

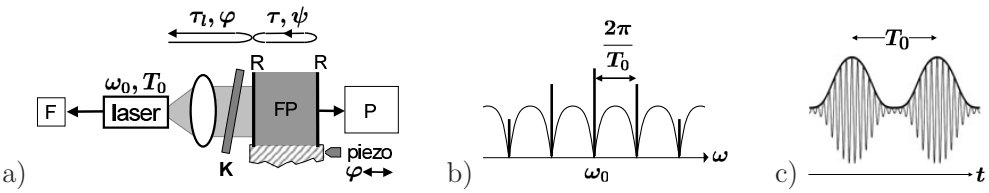

Fig. 2. a) The control setup: laser coupled to a plane FP glass etalon via a collimating lens. ω_0, T_0: optical frequency and pulsation period of the target state (ω_0 belongs to a prominent line in the optical comb), $R, \tau, \psi = \omega_0\tau$ are reflectivity, round-trip time, and optical phase shift of the FP, respectively, $K, \tau_l, \varphi = \omega_0\tau_l$ are feedback gain, round-trip time, and phase shift between laser and FP, respectively. K and φ are adjusted by a variable neutral density filter and a piezo positioning, respectively. F: emission coupled into an optical fiber for further analysis. P: power measurement by infrared photo diode. b) Schematic optical spectra of FP reflectivity (thin) and of a resonant target state (bold). c) Scheme of a possible target state in time domain. Thin: full amplitude $\mathcal{E}(t)$. Bold: slow amplitude $|E(t)|$.

target states it holds $E(t + T_0) = E(t)$ and the complex amplitude returning from the FP to the laser is [8]

$$E_b(t) = Ke^{-i\varphi} \sum_{n=0}^{\infty} (Re^{-i\psi})^n \left[e^{-i\psi} E(t_{n+1}) - E(t_n)\right] \text{ with } t_n = t - \tau_l - n\tau. \quad (3)$$

Losses in the FP and dispersion are omitted for clarity. $K > 0$ comprises all losses between laser and FP including the factor $\sqrt{R}$ for a single reflection. Compared to the standard control force (1) of TDFC, E plays the role of s and several additional parameters appear. The summation over the number n of round trips in the FP corresponds to the well-established extended time-delay autosynchronization (ETDAS) version of conventional TDFC [30], here with complex memory parameter $Re^{-i\psi}$. Since the arguments of the two subtracted amplitudes differ by τ in every order n, integer τ/T_0 and $e^{-i\psi} = 1$ ensure noninvasive feedback. All time arguments τ_n in the sum are shifted by the latency time τ_l. It is known [2,31,32] that a too large latency overrules τ weakening the ability of control. In the experiments, geometrical constraints set a lower limit of $\tau_l \approx 60\,\text{ps}$ which is of the order of τ and thus not yet critical.

The phase shift φ is also not present in conventional TDFC. It makes the total control gain $Ke^{-i\varphi}$ a complex quantity. Its variation over a period of 2π involves thus a sign change of the control force implying a finite φ-range where optical TDFC is possible. To find these ranges in experiment, the distance between laser and FP is systematically varied by a piezo actor with subwavelength precision. Obviously, extreme stability of the whole setup on this scale is a prerequisite of all measurements. Another challenge of the experiments is that the parameters ω_0 and T_0 of the unstable target state are unknown in the beginning. Specific iteration procedures have therefore been developed to meet the conditions $\tau = T_0$ and $e^{-i\psi} = 1$ when targeting control. Details are described separately for unstable steady states [7] and unstable pulsations [9]. The questions why and in which ranges of control parameters φ, K, and R noninvasive feedback can stabilize these types of target states will be a focus of the theoretical sections below.

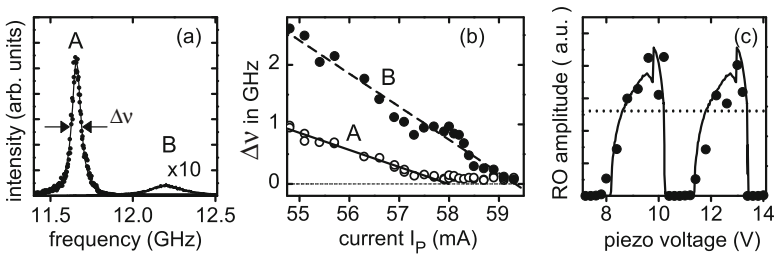

Fig. 3. Optical TDFC of unstable steady states of an ITL. (a) Typical power spectra beyond the Hopf bifurcation of RO without (A) and with (B) control. (b) Line width as a function of I_P without (A) and with (B) control. (c) Peak height versus the piezo voltage used for tuning the latency phase φ. Two periods of φ are depicted. Circles: experiment, lines: simulation, each normalized to mean power emitted by the free-running ITL (dotted line). In all measurements $I_1 = 30\,\mathrm{mA}$, $I_2 = 45\,\mathrm{mA}$, $\tau \approx 38.5\,\mathrm{ps}$, $\tau_l \approx 120\,\mathrm{ps}$, $R = 0.76$, $K \approx 0.04$. In (a,c) $I_\mathrm{P} = 58.5\,\mathrm{mA}$.

4 Control of unstable steady states

Stabilization of steady-state operation of lasers is in general of high practical relevance [33,34]. This Section summarizes the implementation of optical TDFC for this purpose [7] as well as the theoretical approaches accounting for the specifics of semiconductor lasers [8,14]. We consider a Hopf bifurcation, where the relaxation oscillation (RO) by which the laser approaches steady output becomes undamped and a self-pulsation of RO type is born. We start with an experimental example followed by the theoretical analysis.

4.1 Experiment

The Hopf bifurcation of the free-running ITL is identified from RF spectra using current I_P as bifurcation parameter. Noise driven RO are manifested in the RF spectrum by a peak at $1/T_0 \approx 12\,\mathrm{GHz}$ (e.g., peak B in Fig. 3(a)). The zero of the linear decrease of the width of this noisy precursor marks clearly the bifurcation (curve A in Fig. 3(b)) [35]. The precursor mutates here continuously into a narrow line of a noise-broadened RO self-pulsation (peak A in Fig. 3(a)).

Path-following is applied to attain noninvasive control. The ITL is first operated in CW just before the Hopf bifurcation. In order to increase the damping of the RO, the control parameters are chosen as follows. The value of τ is not critical in this case, $\tau \approx T_0/2$ is generally expected to be optimum [2] (see, however, Sec. 4.2 below). Suitable values of R and K are taken from device-realistic simulations [8,23]. To achieve resonance $e^{-i\omega_0\tau} = 1$, the wavelength of the laser is moved by adapting its temperature T until transmission through the etalon is maximum. The required temperature change is far below 1 K and does not affect the essential characteristics of the Hopf bifurcation[2]. Finally, the latency phase φ is used to suppress the RO peak as much as possible. The CW state is then tracked in small I_P-steps through the bifurcation, always readjusting T and φ to maximize FP transmission and damping. With this procedure, the bifurcation point is indeed distinctly shifted to higher phase

[2] The thermal shift of $\omega_0/2\pi$ is about $-20\,\mathrm{GHz/K}$. To correct the maximum possible distance to resonance $1/T_0 \approx 12\,\mathrm{GHz}$ this requests only 0.6 K temperature change. The variations of $\omega_0/2\pi$ with the bifurcation parameter I_P in Fig. 3(b) remain far below 10 GHz and, thus, request much smaller temperature corrections.

currents relative to the solitary ITL (full circles in Fig. 3(b)). As a result of inevitable external and internal noise, there is still a residual RO feature present under control, but its height is suppressed by orders of magnitude (Fig. 3(a)). The control signal is at least three orders of magnitude below the level of the laser emission. The control has therefore indeed noninvasive character. Figure 3(c) displays the variation of the RO peak height as a function of φ, represented by the voltage at the piezo actor. Cyclic behavior directly demonstrates the genuine role of the feedback phase φ in all-optical TDFC. The control domain expands over about 30–40 % of a period, in reasonable agreement with simulations on a full device level detailed in Ref. [8].

4.2 Theory

In the previous Section, we have demonstrated in an experiment that CW output of a laser, which undergoes a Hopf bifurcation towards undamped relaxation oscillations (RO), can be stabilized by all-optical control. From a theoretical perspective, this task translates to analyzing the influence of time-delayed feedback on the local stability of the lasing steady state. Global stability issues such as multistability or hysteresis can also be relevant in optical systems. However, their treatment is beyond the scope of this review. We will discuss some global aspects of the considered laser model in Sec. 4.3.

This Section provides a systematic theoretical framework for the experimental configuration used in this article. We will present a mathematical description for the control of unstable steady-state operation of semiconductor lasers [14]. We aim for a simple, yet sophisticated model that takes into account both dynamic details of an ITL introduced in Sec. 2 and physical aspects of all-optical time-delayed feedback (See Eq. (3) in Sec. 3). To meet these requirements, we utilize a modification of a standard laser model, i.e., the Lang-Kobayashi equations [36], consisting of ordinary differential equations and additional delayed feedback terms as described below. This level of description fills the gap between traveling wave equations [7,8] and generic two-dimensional fixed-point models [2,13]. Traveling wave equations enable detailed, spatially resolved device simulation, but are not feasible for an analytical treatment. Use of the generic normal form of an unstable focus supposes that the purely optical control force is tangent to the two-dimensional center manifold of the Hopf bifurcation. This is not the case in the considered relaxation oscillations, which are due to the interplay of carrier inversion and optical intensity.

Previous work involving a similar model hierarchy focused on the bifurcation analysis of external cavity modes due to a Fabry-Pérot resonator (FP) [10], but considered a stable single-mode laser with overall damped relaxation oscillations. Our type of laser is known to exhibit undamped RO. We will include its dynamic properties via an internal passive dispersive gain function $k(n)$ in Eq. (4b) below. This gain function leads to a destabilization of the CW lasing steady state [37]. Our main finding is that local stabilization of this fixed point can be achieved via all-optical feedback control by a FP. We emphasize that our result is valid for many lasers operated close to a Hopf bifurcation. In this sense, the considered model is paradigmatic.

A semiconductor laser with feedback from a conventional mirror can be described by the Lang-Kobayashi equations [36]. Other types of feedback have also been investigated [29,38,39]. As in previous Sections, we consider feedback that is generated in an all-optical setup realized by a FP [7,10] (see Fig. 2(a) for a schematic diagram of the system). The general form of FP feedback is given by Eq. (3).

We investigate a modification of the dimensionless Lang-Kobayashi equations appropriate for multisection semiconductor lasers with an internal passive dispersive reflector and all-optical feedback. This combines different Lang-Kobayashi-type

models of Refs. [10,12,14,37]:

$$\frac{\mathrm{d}}{\mathrm{d}t}E = \frac{1}{2}(1+i\,\alpha)\,n\,E + E_b(t) + F_E(t), \tag{4a}$$

$$T\frac{\mathrm{d}n}{\mathrm{d}t} = p - n - (1+n)k(n)\,|E|^2 \quad \text{with} \quad k(n) = k_0 + \frac{AW^2}{4\,(n-n_0)^2 + W^2}, \tag{4b}$$

where E is the complex electric field amplitude, n is the carrier density in excess of the threshold density, α is the linewidth enhancement factor, p is the excess pump injection current, T is the ratio between the carrier lifetime ($\tau_c \approx 10^{-9}\,\mathrm{s}$) and the photon lifetime ($\tau_p \approx 10^{-12}\,\mathrm{s}$). For details see Ref. [40]. $E_b(t)$ denotes the feedback term (3) describing the FP resonator. F_E is a white noise term describing the spontaneous emission. The effect of noise due to spontaneous emission will be discussed in detail later in Sec. 6 and is neglected in this Section.

The gain function $k(n)$ models the internal dispersive feedback from the Bragg grating as introduced in Ref. [37]. A denotes the height, W is the width, and n_0 is the position of the resonance. The parameter k_0 is chosen such that $k(0) = 1$ at the laser threshold. Such a laser structure exhibits more complex dynamic behavior including self-sustained relaxation oscillations (intensity pulsations) generated by Hopf bifurcations, as has been shown in the framework of traveling wave laser models [7,23]. In our simulations, we use the following parameters, which were chosen close to the values of Ref. [37]: $\alpha = 5$, $T = 500$, $p = 1.8$, $A = 1$, $W = 0.02$, $n_0 = -0.033933$, and $k_0 = 0.993075$.

Since the FP feedback is given by Eq. (3) with $\psi = 2\pi$, the control parameter space consisting of K, τ, R, φ, and τ_l is five-dimensional. To visualize the domain of control, we consider two-dimensional sections of this parameter space. In this paper, we focus on the influence of the control phase φ on the stability of the fixed point. Detailed studies on the influence of the latency time τ_l exist for normal forms [2,13,31,32] and Lang-Kobayashi equations [14]. Here, we set $\tau_l = 0$ for simplicity.

To investigate the stability of the CW laser emission, we will first consider the system without the feedback term. Next to a trivial, non-lasing fixed point at ($n = p, E = 0$), there exists another lasing steady state at ($n = 0, E = \sqrt{p}e^{i\phi}$).The phase of the electric field can be arbitrarily fixed to $\phi = 0$, such that $e^{i\phi} = 1$ (solitary laser mode). This leads to symmetry breaking of the rotational (S1) symmetry of Eqs. (4) with respect to complex E. Using the abbreviations

$$\Gamma = \frac{1}{T}\left[1 + p\left(1 + \left.\frac{\mathrm{d}k}{\mathrm{d}n}\right|_{n=0}\right)\right] \quad \text{and} \quad E(t) = \sqrt{T}\,[E_0 + x(t) + iy(t)]$$
$$\text{with} \quad E_0 = \sqrt{\frac{p}{T}} \tag{5}$$

with real-valued x and y, the fixed point is located at ($n = 0, x = 0, y = 0$). Using parameters as above, this yields $E_0 = 0.06$ and $\Gamma = -0.01$. A linearization around this point leads to the following system of equations:

$$\begin{pmatrix}\dot{n}(t)\\ \dot{x}(t)\\ \dot{y}(t)\end{pmatrix} = \begin{pmatrix}-2\Gamma & -4E_0 & 0\\ E_0 & 0 & 0\\ -E_0\alpha & 0 & 0\end{pmatrix}\begin{pmatrix}n(t)\\ x(t)\\ y(t)\end{pmatrix} - K\begin{pmatrix}0 & 0 & 0\\ 0 & \cos\varphi & \sin\varphi\\ 0 & -\sin\varphi & \cos\varphi\end{pmatrix}$$
$$\times \sum_{m=0}^{\infty} R^m \begin{pmatrix}0\\ x(t-m\tau) - x(t-(m+1)\tau)\\ y(t-m\tau) - y(t-(m+1)\tau)\end{pmatrix} \tag{6}$$

with an appropriate time scale transformation $t = sT/(2\tau_c) = s/(2\tau_p)$ with respect to the physical time s to eliminate the parameter T. Following this scaling, the feedback gain K of Eq. (3) has to be transformed accordingly with respect to the experimentally used values. From this set of equations one can clearly see the proper description of a physically relevant, all-optical feedback. The FP feedback term yields a control signal that is applied to the real and imaginary parts of the complex electric field only, while the feedback does not enter the equation of the carrier density n. This carrier equation is crucial to grasp the full dynamics of the RO, which happen in the $(n, |E|)$-plane. This aspect cannot be treated accurately within a generic two-dimensional model of an unstable focus [2,7,13].

In order to investigate the stability of the fixed point in the uncontrolled system, we consider the case $K = 0$. Then, the eigenvalues $\Lambda \in \mathbb{C}$ are given by $\Lambda = 0$ and $\Lambda = -\Gamma \pm i\sqrt{4E_0^2 - \Gamma^2}$. The Goldstone mode $\Lambda = 0$ does not contain information about the stability of the fixed point and is only present due to the rotation symmetry. Therefore, only the second solution is of interest. Note that the imaginary part $\Omega_0 = 2\pi/T_0 = \sqrt{4E_0^2 - \Gamma^2}$, which corresponds to the frequency of the relaxation oscillation, exists only for $|2E_0| > |\Gamma|$. Under this condition the fixed point is a focus. Since $-\Gamma$ is the real part of the eigenvalue Λ, the focus is stable for any $\Gamma > 0$ and unstable otherwise. The case $\Gamma = 0$ corresponds to the Hopf bifurcation generating the RO in the experiment. Starting with an unstable focus ($\Gamma < 0$), we investigate the effects of the extended time-delayed feedback control $E_b(t)$ given by Eq. (3) on the stability of the fixed point in the following.

We include the time-delayed control term with properly rescaled feedback strength K in the linearized equations. Using an exponential ansatz $\exp(\Lambda t)$ for all three variables x, y, and n leads to the characteristic equation

$$0 = (2\Gamma + \Lambda)\left[\left(K\frac{1-e^{-\Lambda\tau}}{1-Re^{-\Lambda\tau}}\right)^2 + \Lambda^2 + 2\Lambda K\frac{1-e^{-\Lambda\tau}}{1-Re^{-\Lambda\tau}}\cos\varphi\right]$$
$$+4E_0^2\left(\Lambda + K\frac{1-e^{-\Lambda\tau}}{1-Re^{-\Lambda\tau}}\cos\varphi + \alpha K\frac{1-e^{-\Lambda\tau}}{1-Re^{-\Lambda\tau}}\sin\varphi\right). \quad (7)$$

Although this transcendental equation has an infinite number of roots, we locate only the eigenvalue with the largest real part, which determines stability, by a root-finding algorithm. Note that the boundary of the control domain can be obtained analytically in the special case of $\varphi = 0$ [14]. Here, however, we are interested in effects of a non-vanishing control phase. Therefore, the domain of control will be investigated in the (K, τ)- and (K, R)-plane with φ as an additional parameter.

In Fig. 4(a), (b), (c), and (d), the domain of control is shown in the (K, τ)-plane for different values of the phase $\varphi = 0$, $\pi/16$, $\pi/8$, and $3\pi/16$, respectively. The grayscale (color code) denotes the largest real part of the eigenvalues and is therefore a measure of stability. Note that only values of $\mathrm{Re}(\Lambda) < 0$ are plotted, thus the shaded regions correspond to a stable lasing fixed point, i.e., a stable CW output. The control domains form tongues separated by (white) regions of no control around $\tau = mT_0$ with m integer and $T_0 = 2\pi/\sqrt{4E_0^2 - \Gamma^2}$, just as in the generic model studied in Refs. [2,13]. It can be seen that the domain of control shrinks with increasing phase, while it is shifted to larger values of the feedback gain K. For the case of vanishing R, i.e., single reflection in the FP, it was shown previously that the optimum time delay is given by $\tau_{opt} = T_0/2$ which yields $\tau_{opt} = \pi/\sqrt{4E_0^2 - \Gamma^2} \approx 26$ for the Lang-Kobayashi model with our parameters [14]. In Fig. 4(a), (b), (c), and (d), however, we used $R = 0.7$. Hence, the domains of control are distorted to smaller time delays. This has the important, experimental consequence that higher reflectivity of an FP in experiments allows us to use smaller etalons.

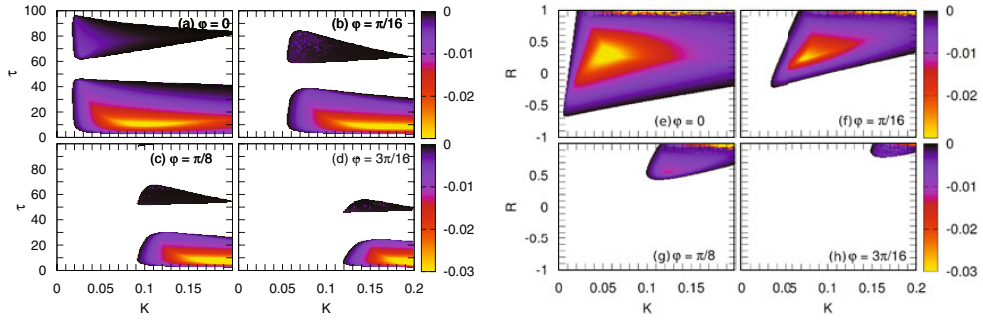

Fig. 4. Domain of control according to Eq. (7) for different values of φ: (left) in the (K, τ)-plane for fixed $R = 0.7$, (right) in the (K, R)-plane for fixed optimum time delay $\tau = 26$. The grayscale (color code) denotes the largest real part $\mathrm{Re}(\Lambda)$ of the eigenvalues Λ, only negative values are plotted. Other parameters: $\Gamma = -0.01$, $E_0 = 0.06$, $\alpha = 5$, $T = 500$, and $p = 1.8$.

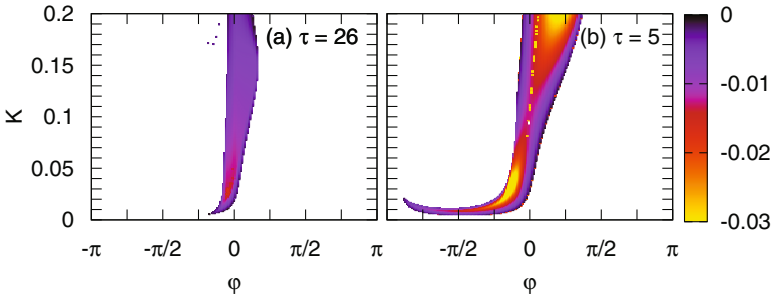

Fig. 5. Domain of control in the (K, φ)-plane for different values of τ. The grayscale (color code) denotes the largest real part $\mathrm{Re}(\Lambda)$ of the eigenvalues Λ, only negative values are plotted. Panels (a) and (b) correspond to $\tau = 26$ and 5, respectively. Other parameters as in Fig. 4.

To show the dependence of the control on R, we display the domains of control in the (K, R)-plane for different values of the phase $\varphi = 0$, $\pi/8$, $\pi/4$, and $3\pi/8$ in Fig. 4 (e)–(h), respectively. The time delay is fixed as $\tau = 26$. One can see that large R values correspond to larger intervals of possible feedback gains K. In addition, the domain of control in the (K, R)-plane has maximum size for $\varphi = 0$ for this choice of the time delay τ, while for larger values of the phase φ stability is then only achieved in a small region at large values of K and R. In an experiment, where R and τ are fixed parameters determined by the FP, proper adjustment of the feedback phase φ is crucial to achieve stabilization for a given experimental setup.

To elaborate the dependence of the domain of control on the choice of the phase φ further, we investigate the domain of control in dependence of the feedback gain K and the feedback phase φ in Fig. 5 for two different values of the time delay. For $\tau = 26$ (panel (a)), the optimum phase is located at slightly negative values for small values of the feedback gain, while the optimum phase changes its sign and is located at small positive values of φ for larger K. For the case of $\tau = 5$, which is depicted in panel (b), stability is overall enhanced drastically. Control is possible even for a small value of φ below $-\pi/2$, if the feedback gain is tuned exactly to the small range of $K \approx 0.01$, while for larger feedback gain, the size of the domain of control is increased compared to $\tau = 26$. The shape of the control domain in Fig. 5 is markedly different

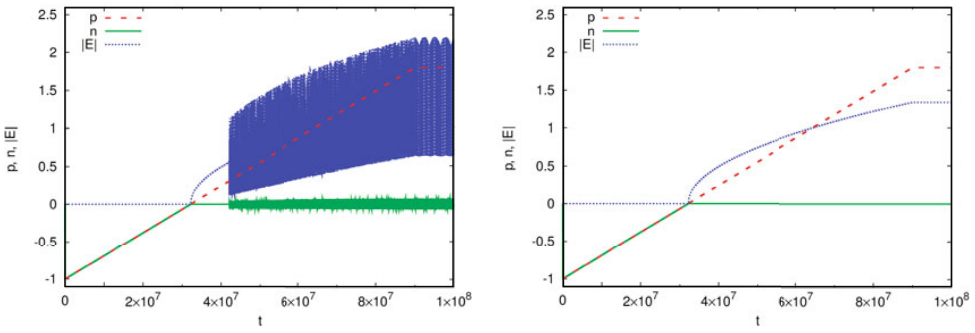

Fig. 6. Dynamics of the system during a turn-on process in dimensionless time units rescaled by the photon lifetime: (a) without feedback ($K = 0$), (b) with feedback ($K = 0.1$, $\tau = 26$, $R = 0.7$, and $\varphi = 0$). The dashed (red), solid (green), and dotted (blue) curves correspond to the injection current p, the carrier inversion n, and the absolute value of the electric field $|E|$, respectively. Other parameters as in Fig. 4.

from that in a generic normal form model of an unstable focus (see Figs. 6(c) and 7(c) in Ref. [13]), but appears to be in line with full device simulations within a traveling-wave model [8]. Furthermore, it can be shown that the lasing fixed point undergoes a transcritical bifurcation on the left boundary and thus, loses its stability. Due to the Goldstone mode $\Lambda = 0$ is always a solution of Eq. (7). At the transcritical bifurcation of periodic orbits $\Lambda = 0$ has to be a two-fold eigenvalue. Thus, the characteristic Eq. (7) and its derivative have to be zero, which is fulfilled if the coefficient in a linear expansion of Eq. (7) vanishes. The left boundaries in Figs. 5(a) and (b) are then given by $K = (R-1)\,/\,[\tau\,(\alpha\cos\varphi + \sin\varphi)]$. This result underlines the importance to analyze a physically relevant feedback scheme in a simple but sophisticated model.

The theoretical results obtained in this Section complement the experimental realization of the stabilization of the lasing fixed point (CW emission) in a semiconductor laser. By a stability analysis of this fixed point under the influence of the delayed feedback, we were able to predict the possible extent of the parameter space that leads to stability, which matches the experimental findings.

4.3 Turn-on dynamics

In all preceding considerations, the effect of time-delayed feedback control on the stability of the lasing fixed point was investigated only locally, since the system was linearized around the fixed point. Besides the fixed point associated with CW emission, the model 4 has a limit cycle in the $(n, |E|)$-plane already in the absence of control. This limit cycle corresponds to undamped relaxation oscillations (intensity pulsations). The amplitude of this limit cycle, which is born by a subcritical Hopf bifurcation at $\Gamma = 0$, depends on the choice of the parameters. For the chosen set of parameters, the limit cycle is located around $(n = 0, |E| = 1.342)$. In an experiment, the case may be of interest where the feedback is activated when the laser is operating at this limit cycle of relaxation oscillations. Therefore, for numerical simulations we choose initial conditions on this limit cycle: $E(t = 0) = -0.731767 - i\ 0.016891$, which corresponds to $x(0) = -0.0927256$ and $y(0) = -0.00075538$. The initial values of the reduced carrier density is chosen as $n(0) = -0.037433$.

Depending on the feedback gain K and the time delay τ, the system exhibits diverse scenarios ranging from limit cycles to chaotic attractors. Note that the lasing fixed point (solitary laser mode) at $n = 0$ may be stable for values of $K > 0$ according

to the linear stability analysis, thus there exists multistability between CW laser emission and (periodic or chaotic) intensity pulsations. It depends upon the initial conditions which attractor is asymptotically reached. If the initial condition is chosen in the vicinity of the fixed point, where the linearization is valid, time-delayed feedback control still works to stabilize CW emission. This can be achieved, for instance, by first operating the laser below the Hopf bifurcation and then gradually increasing the pump current, and hence Γ.

We have simulated an adiabatic turn-on scenario [14] that is similar to the experimental technique used in Sec. 4.1, where the ITL was first operated below the Hopf bifurcation and then driven through the bifurcation in tiny steps of the bifurcation parameter I_{P}. As a result of the slowly increasing instability the feedback is able to keep the dynamics in the very vicinity of the lasing fixed point. Even with a small amount of noise this behavior is expected to persist, since the basin of attraction of the fixed point is finite.

The turn-on scenario is depicted in Fig. 6(a) for the case of no control. The laser is first operated below the laser threshold with the injection current chosen as $p = -1$. With initial conditions chosen arbitrarily as $x = y = 10^{-6}$ and $n = 0$ the laser relaxes into the non-lasing fixed point $(n = p, E = 0)$. The injection current is then linearly increased until the value of $p = 1.8$ is reached. This final value was also used in Figs. 4 and 5. Passing the laser threshold at $p = 0$, non-lasing and lasing fixed points change stability, thus the system swaps to the lasing fixed point with $n = 0$ and nonzero E. Increasing the current further beyond the value of $p = 0.3$, the lasing fixed point becomes again unstable due to the internal dispersive feedback. Reaching $p = 1.8$, the system resides in the limit cycle. The full turn-on process from $p = -1$ to 1.8 takes 9×10^7 in the rescaled time units used in these simulations. Assuming a photon lifetime of the order of $\tau_p \approx 10^{-11}$ s, this would relate duration of the turn-on ramp of 1.8 ms. See also the scaling of Eqs. (6).

We now consider the system in the presence of control. For experimental feasibility the feedback is active during the full turn-on process. We consider an exemplary case with $\tau = 26$, $K = 0.1$, $R = 0.7$, and $\varphi = 0$. The dynamics during the turn-on process is shown in Fig. 6(b). It can be seen that the system remains in the vicinity of the lasing fixed point even beyond the point $p = 0.3$. This is achieved since the feedback is already active as the system passes this onset of instability. As the system is thereby always kept near the fixed point, the results of the linear stability analysis presented above can be applied here. Another evidence for the success of the control is the fact that after the turn-on process the control force vanishes.

The slow ramping of system parameters such as the injection current is a well-established experimental procedure to reach an operating point of the laser in cases where the basin of attraction of the corresponding steady state is rather small and, thus, local stability is fragile. Then, sudden or too fast turn-on of the laser might trigger unwanted RO, which are also present in the system due to multistability even in the absence of FP feedback. However, this global stability effect can be overcome. The desired operating point can be reached if the feedback enhances the local stability of the CW lasing steady state. In addition to the stabilization of the lasing fixed point, we focus on the stabilization of periodic orbits (intensity pulsations) embedded in a chaotic attractor in the next Section.

5 Chaos control

Chaos in semiconductor lasers has mostly to be avoided in order to maintain stable operation. On the other hand, secure communication by using chaotic light has become an issue of growing interest [21, 41–43]. In this context, all-optical chaos control

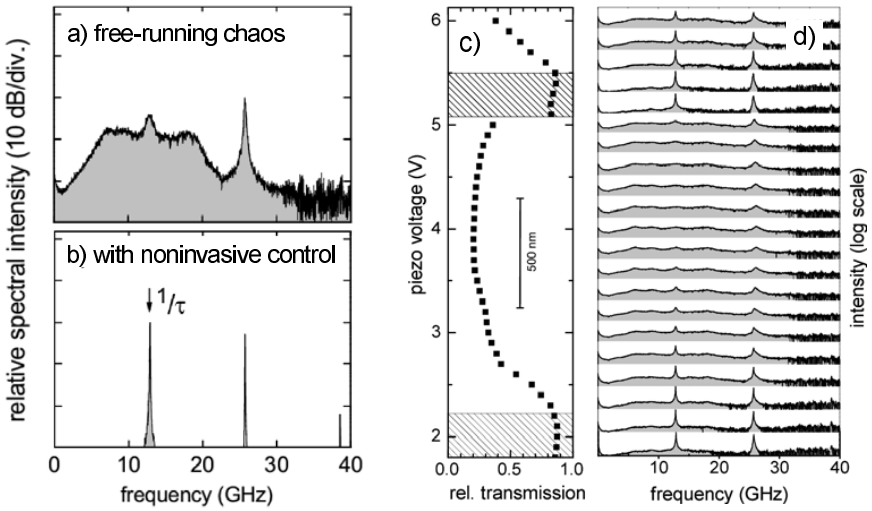

Fig. 7. All-optical TDFC experiment. (a,b) Stabilization of a periodic pulsation embedded in the chaotic regime. The height of the strongest feature in all spectra is arbitrarily scaled. Note the log scale. (c,d) Effect of latency phase φ on control. φ is tuned via the voltage at the piezo actor (cf. Fig. 2(a)). (c): Power transmitted through the FP (horizontal axis) versus piezo voltage (vertical scale). The power is given relative to the laser output. Shaded areas mark the regions of control. (d): Power spectra corresponding to selected piezo voltages in the left part. Parameter: $I_{1,p,2} = (57.0, 65.1, 74.4)\,\mathrm{mA}$, $\tau = 77\,\mathrm{ps}$, $K \approx 0.03$, $R = 0.76$.

becomes important, i.e. noninvasive stabilization of unstable periodic pulsations embedded in the chaotic attractor. This goal has been met by means of optical TDFC using an ITL in the setup of Fig. 2(a) [9]. Operating in the ps-domain, this is the fastest chaos ever controlled in a practical device.

The free-running ITL is set to chaotic operation with the broad power spectrum shown in Fig. 7(a). Two weak features superimposed to the otherwise broad power spectrum are fingerprints of a frequently visited unstable pulsation (unstable periodic orbit or UPO) in the chaotic attractor. To achieve noninvasive chaos control is much more difficult than the previous control of steady states. The minima of the FP reflectivity spectrum have to match not only to a single spectral line, but to all Fourier components of the targeted UPO, cf. Fig. 2(b). The difficulty is twofold: neither the carrier frequency ω_0 nor the period T_0 of the UPO are precisely known in advance. An essential advantage of the ITL in this regard is that ω_0 and T_0 can be tuned rather independently through the device temperature and the currents on the laser sections. This enables us to satisfy both requirements with a fixed etalon. Its round trip frequency $1/\tau$ is set to the weak feature at 13 GHz expected to reveal an UPO. Noninvasive control is achieved by an iterative procedure. First, R and K are set to appropriate estimates. Second, φ is varied over more than one period and series of spectra similar to Fig. 7(d) are recorded. Third, that φ is selected where the targeted UPO feature is most prominent. Forth, transmission through the FP is maximized by slight adaptions of temperature and currents. The whole procedure is successful if the target peak is more than 30 dB above background and the feedback power reinjected in the laser is more than 30 dB below the laser output. Otherwise previous steps are repeated with slightly different parameters. Figure 7(b) demonstrates an example where a nearly perfect periodic regime is recovered. Finally, by removing the FP, it has been checked that the change of the device operation point did not leave the chaotic domain of the free-running laser.

Figure 7(d) assembles a series of measurements in the chaotic regime where the position of the FP is moved in small steps of about 47 nm. The sub-ps alteration of τ_l itself is unimportant, but φ changes over one period when the total translation equals the wavelength. Periodicity, both in the FP transmission as well as in the power spectra, is clearly recognizable. The range of control, identified by a transmission close to unity and sharp peaks in the power spectrum, is about 15% of the period. Again, this is in reasonable agreement with simulations, which also provide control domains with respect to other parameters [9], but are beyond the scope of this paper. Out of the control ranges in Fig. 7(c), the power spectra are even less structured than in the uncontrolled device indicating an increased irregularity of the emission. Such behavior might be interesting for applications demanding an extremely flat spectral response.

6 Suppressing noise-induced oscillations

The noninvasive control of the different target states considered so far is based on a common mechanism: their deterministic local stability is changed without changing themselves. Now we consider states which are deterministically stable without control, and investigate the effect of TDFC upon purely noise-induced oscillations. These noise-induced oscillations are a widespread phenomenon and appear, for instance, in lasers [44–48], chemical reaction systems [49], semiconductor devices [50,51], neurons [52], and many other systems. While previous studies have shown that the delayed feedback method can control the main frequency and the correlation time and thus the regularity of noise-induced oscillations in simple systems [53–59] as well as in spatially extended systems [60–62], and deteriorate or enhance stochastic synchronization of coupled systems [63–65], in this Section we focus on the *suppression* of noise-induced oscillations which are omnipresent in real lasers. We analyze the mean amplitude (or, more generally, the covariance) of the oscillations and show that time-delayed feedback control can decrease the mean oscillation amplitude for appropriately chosen delay time, and thus suppress the oscillations. In Section 4, we have already seen that noninvasive control of the steady state sharpens the noisy precursor of a Hopf bifurcation. In what follows, we present the theoretical prediction of this effect [12] supplemented with confirming experimental data.

6.1 Theory

We investigate model equations 4 with $k(n) \equiv 1$, i.e., a usual semiconductor laser without the dispersive reflector discussed above. We now consider nonzero spontaneous emission noise F_E and use a feedback term of the form Eq. (3) with $\psi = 0$, $\varphi = 0$, $\tau_l = 0$, and $R = 0$ corresponding to noninvasive feedback from a FP cavity with low reflectivity, where multiple reflections can be neglected.

This choice is inspired by the stabilization of unstable fixed points, where $\varphi = 0$ leads to the largest domains of stability (see Fig. 4). For the analysis of the phase dependence in the deterministic case, see Sec. 4.2 and [7,13,14]. We consider small feedback strength K, so that the laser is not destabilized by delay-induced bifurcations and only one mode exists. A sufficient condition [10] is that $K < K_c = 1/(\tau\sqrt{1+\alpha^2})$.

The noise term F_E in Eq. (4a) arises from spontaneous emission, and we assume the noise to be white and Gaussian $\langle F_E \rangle = 0, \langle F_E(t)\,\overline{F_E(t')}\rangle = R_{sp}\delta(t-t')$ with the spontaneous emission rate $R_{sp} = \beta(n+n_0)$, where β is the spontaneous emission factor and n_0 is the threshold carrier density. Without noise the laser operates in a stable steady state corresponding to continuous wave emission. We transform the

complex field Eq. (4a) into equations for intensity I and phase ϕ using $E = \sqrt{I}\, e^{i\phi}$:

$$\frac{\mathrm{d}}{\mathrm{d}t} I = n\, I - 2K \left[I - \sqrt{I}\sqrt{I(t-\tau)}\, \cos\left(\phi(t-\tau) - \phi\right) \right] + R_{sp} + F_I(t),$$
$$\frac{\mathrm{d}}{\mathrm{d}t} \phi = \frac{1}{2}\alpha\, n + K\, \sqrt{I(t-\tau)/I}\, \sin\left(\phi(t-\tau) - \phi\right) + F_\phi(t). \tag{8}$$

The noise terms in these coordinates are determined by $\langle F_I(t)\, F_I(t')\rangle = 2R_{sp}\, I\, \delta(t-t')$ and $\langle F_\phi(t)\, F_\phi(t')\rangle = R_{sp}/(2I)\, \delta(t-t')$ and all other correlation and mean values being zero.

Setting $\mathrm{d}I/\mathrm{d}t = 0$, $\mathrm{d}n/\mathrm{d}t = 0$, $\mathrm{d}\phi/\mathrm{d}t = \text{const}$, $K = 0$ and replacing the noise terms by their mean values, gives a set of equations for the mean steady state solutions I_*, n_*, and $\phi = \omega_* t$ without feedback (the solitary laser mode). Our aim is now to analyze the stability (damping rate) of the steady state. A high stability of the steady state, corresponding to a large damping rate, will give rise to small-amplitude noise-induced relaxation oscillations whereas a less stable steady state gives rise to stronger relaxation oscillations. Linearizing Eqs. (8) around the steady state $X(t) = X_* + \delta X(t)$ with $X(t) = (I, \phi, n)$ gives

$$\frac{\mathrm{d}}{\mathrm{d}t} \delta X(t) = U\, \delta X(t) - V\, [\delta X(t) - \delta X(t-\tau)] + F(t). \tag{9}$$

Here, U is the Jacobian matrix of the right-hand side of Eqs. (8) without control ($K = 0$) and $V = \mathrm{diag}(K,\, K,\, 0)$, where diag(...) denotes a 3×3 diagonal matrix, and $F = (F_I,\, F_\phi,\, 0)$. The Fourier transform of Eq. (9) gives $\widehat{\delta X}(\omega) = M(\omega)\, \widehat{F}(\omega)$ with $M(\omega) = [i\omega - U + V\,(1 - e^{-i\omega\tau})]^{-1}$. Using the covariance matrix (see [12] for details) $\langle \widehat{F}(\omega) \widehat{F}(\omega')^\dagger \rangle = C\delta(\omega - \omega')$ with $C = \mathrm{diag}(2R_{sp}I_*,\, R_{sp}/2I_*,\, 0)/2\pi$ of the noise we can calculate the matrix-valued power spectral density

$$S(\omega) = M(\omega)\, C\, M(\omega)^\dagger. \tag{10}$$

This is an analytic expression for the power spectral density in the linear regime. The diagonal elements of the matrix S are the power spectral densities of the intensity $S_{\delta I}$, the phase $S_{\delta\phi}$, and the carrier density $S_{\delta n}$. The frequency power spectrum is related to the phase power spectrum $S_{\delta\phi}(\omega)$ by [66] $S_{\delta\dot{\phi}}(\omega) = \omega^2\, S_{\delta\phi}(\omega)$.

We shall now investigate how the noise can be controlled by a proper choice of the delay time of TDFC.

The laser parameters we consider in the following are typical values for a single mode distributed feedback laser operating close to threshold [10,66]. Figure 8 displays the intensity and the frequency power spectra for different values of the delay time τ, obtained from simulations of the full nonlinear equations (right) and the analytic results of Eq. (10). All spectra have a main peak at the relaxation oscillation frequency $\Omega_{RO} \approx 0.03$. The higher harmonics can also be seen.

These results can be understood as follows. Spontaneous emission noise excites damped relaxation oscillations between carrier density and intensity, which are manifested as a peak in the intensity power spectrum. For $\tau = 0$ (no control) the peak is large, i.e., the relaxation oscillations are weakly damped. With increasing delay time, the fixed point (focus) becomes more stable and the peak height decreases until it reaches a local minimum at $\tau_{opt} \approx T_{RO}/2 = 2\pi/(2\Omega_{RO}) \approx 100$. For this optimal delay time the steady state is most stable and the relaxation oscillations have a small amplitude, i.e., noise-induced intensity pulsations are suppressed. With further increasing τ the peak height increases again until it reaches approximately its original maximum at $\tau \approx T_{RO}$.

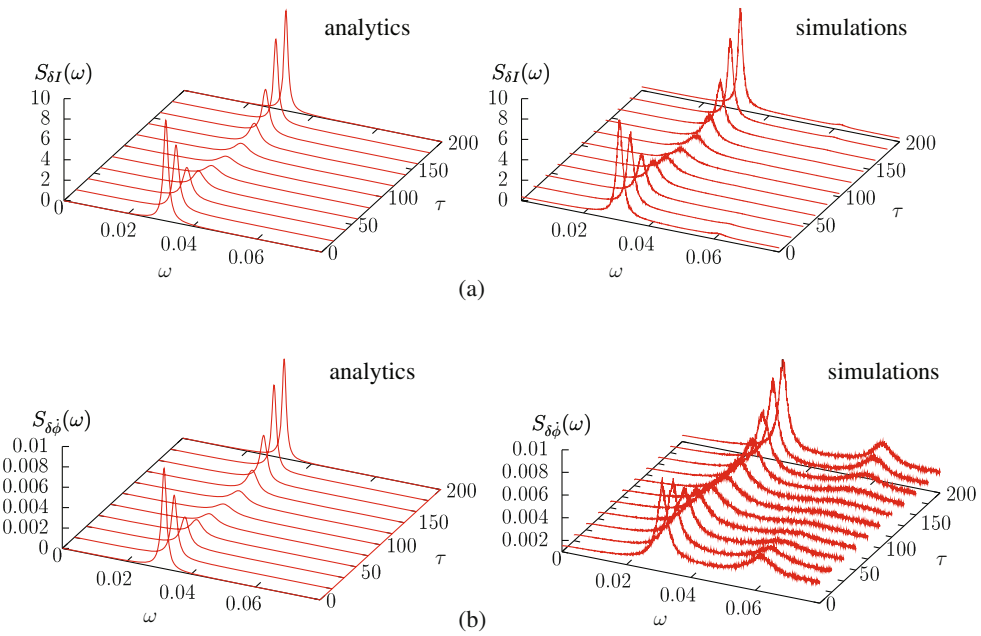

Fig. 8. Numerical and analytical results for the power spectral densities $S_{\delta I}(\omega)$ of the intensity (a) and $S_{\delta\dot{\phi}}(\omega)$ of the frequency (b) for different values of the delay time τ. Parameters: $p = 1$, $T = 1000$, $\alpha = 2$, $\beta = 10^{-5}$, $n_0 = 10$, $K = 0.002$. The relaxation oscillation period for these parameters is $T_{RO} \approx 200$. The optimal value of the delay time is $\tau = T_{RO}/2 \approx 100$ (compare Sec. 4.2). A typical unit of time is the photon lifetime $\tau_p \approx 10^{-11}$ s, corresponding to a frequency of 100 GHz.

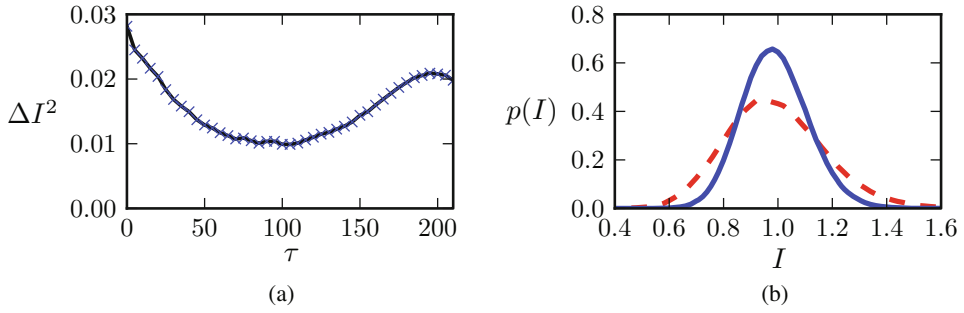

Fig. 9. (a) Variance of the intensity I vs the delay time. (b) Probability distribution of the intensity I with (solid) and without (dashed) the resonator ($\tau = 100$) obtained from simulations. Parameters as in Fig. 8.

Through the α-factor the oscillating carrier density couples into the phase of the electric field (see phase Eq. (8)) and thus causes slight oscillations of the laser frequency with the relaxation oscillation period. This results in a corresponding peak in the frequency power spectrum in Fig. 8. Note that external feedback also has an influence on the optical line width $\Delta\nu$, which is determined by the frequency power spectrum at zero $\Delta\nu = S_{\delta\dot{\phi}}(0)/2\pi$ [66].

Next, we study the variance of the intensity distribution as a measure for the oscillation amplitude $\Delta I^2 \equiv \langle (I - \langle I \rangle)^2 \rangle$. Figure 9(a) displays the variance as a

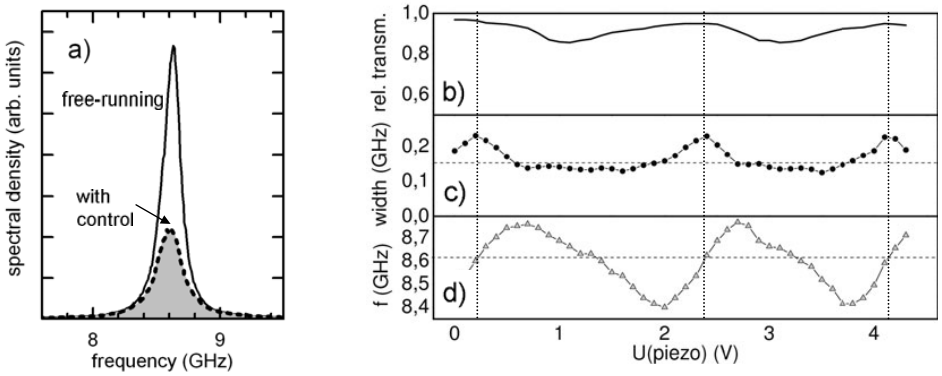

Fig. 10. Control of noise-induced RO. a) Power spectra of RO in the free-running laser (solid) and with resonantly coupled FP (dotted). Parameter: $I_L = 99.9\,\mathrm{mA}$, $I_P = 32\,\mathrm{mA}$, $I_A = 9\,\mathrm{mA}$, $K = 0.03$, $R = 0.5$, $1/\tau = 17.5\,\mathrm{GHz} \approx 2f_0$, φ at optimum (middle vertical line in right panels). b) relative FP transmission, c) RO peak width, and d) RO frequency, vs the piezo voltage U that adjusts the phase φ. Horizontal dotted lines: free-running values. Vertical lines: maximum suppression of RO.

function of the delay time. The variance is minimum at $\tau \approx T_{RO}/2$, thus for this value of τ the intensity is most steady and relaxation oscillations excited by noise have a small amplitude. Note that it is possible to derive analytic results, such as the mean square oscillation amplitude, in a generic normal form model, which gives very good agreement with the numerical results (see Fig. 5(a) in Ref. [12]).

Figure 9(b) displays the intensity distribution of the laser without (dashed) and with (solid) optimal control (compare Fig. 6 in Ref. [12]). The time-delayed feedback control leads to a narrower distribution. While the suppression and widening of the peak in the power spectra indicates that the temporal coherence of the oscillations is controlled, i.e., the correlation time is decreased, a narrowed intensity distribution as shown in Fig. 9(b) corresponds to a decreased amplitude of the intensity fluctuations.

6.2 Experiment

The experiments are performed similarly to those of Sec. 4, now with an AFL to demonstrate device-independence of the control. The device is set to stable CW operation before a Hopf bifurcation, where the noise-induced precursor at $f_0 \approx 8.6\,\mathrm{GHz}$ exceeds distinctly the noise floor in the power spectrum, see solid line in Fig. 10(a). The dotted line is measured after resonantly coupling to a $\tau f_0 = \frac{1}{2}$ etalon and properly adapting φ. Obviously, the noise-induced oscillations are distinctly reduced in agreement with the above theory. The ratio between the two lines compares fairly well with that of the corresponding calculated lines in Fig. 8(a). The first line ($\tau = 0$) belongs to the free-running laser and the middle line $\tau = T_{RO}/2 \approx 100$ corresponds to the controlled line in Fig. 10(a). As in all control experiments discussed so far, the impact of the resonant feedback on the RO line depends sensitively on the latency phase φ. The right panels in Fig. 10 show more than two phase periods. The vertical lines indicate equivalent phases (differing by integer multiples of 2π) where the damping of the RO becomes maximum. The dotted spectrum in panel (a) is measured here. The line width (and thus, the RO damping) is about 1.5 times larger than in the free-running device. In the same points, the transmission through the FP is maximum, i.e. the noise induced motion away from steady state is suppressed without changing this state itself. These results have opened the way for noninvasive control of further

noise effects. Very recently, optical TDFC has succeeded to improve the coherence of self-pulsations and to stabilize bistable states against noise-induced escape [17].

7 Conclusion

In this article we have reviewed recent studies of all-optical time-delayed feedback control. The Pyragas-type control force is provided here by purely optical feedback from an external Fabry-Pérot interferometer. Since this approach needs no demanding and numerically expensive signal processing, it is practically free of any speed limit. This has been experimentally validated on picosecond time scales by controlling steady states, periodic pulsations embedded in chaos, and noise-induced oscillations in multisection lasers as used in optical communication. Concerning theory, we have focused on Lang-Kobayashi type delay-differential equations, which keep the balance between sufficiently complex dynamics of the solitary laser on the one hand, and sufficient simplicity to allow for insight by mathematical analysis on the other hand. The domains of control parameters allowing for stabilization of steady states have been mapped out in good agreement with the experiments. Furthermore, including spontaneous emission as a stochastic force, an analytical expression for the power spectral density is derived, which describes well the experimental control of noise-induced oscillations.

Besides the absence of speed limitations, a sensitive dependence on the optical phase has been identified as the most important feature of optical time-delayed feedback control. On the one hand, this provides a new degree of freedom because the phase shift between laser and interferometer appears as an independent control parameter. On the other hand, the practical applicability is limited for the following two reasons. First, domains of successful control and of failure of control alternate periodically with the wavelength when the distance between laser and interferometer is varied. Second, the interferometer must be exactly resonant with the emission of the laser in the target state. These features require subwavelength stability and addressability of both interferometer position and length, which makes the used external setup expensive, difficult to adjust, and unsuitable for routine applications. We believe, however, that these drawbacks can be overcome by integration of the interferometer on the same chip.

References

1. K. Pyragas, Phys. Lett. A **170**, 421 (1992)
2. P. Hövel, E. Schöll, Phys. Rev. E **72**, 046203 (2005)
3. *Handbook of Chaos Control*, edited by E. Schöll, H.G. Schuster (Wiley-VCH, Weinheim, 2008), second completely revised and enlarged edition
4. D.J. Gauthier, D.W. Sukow, H.M. Concannon, J.E.S. Socolar, Phys. Rev. E **50**, 2343 (1994)
5. C. Bornholdt, J. Slovak, B. Sartorius, Electron. Lett. **40**, 192 (2004)
6. I. Kim, C. Kim, G. Li, P. LiKamWa, J. Hong, IEEE Phot. Technol. Lett. **17**, 1295 (2005)
7. S. Schikora, P. Hövel, H.-J. Wünsche, E. Schöll, F. Henneberger, Phys. Rev. Lett. **97**, 213902 (2006)
8. H.-J. Wünsche, S. Schikora, F. Henneberger, in *Handbook of Chaos Control*, edited by E. Schöll, H.G. Schuster (Wiley-VCH, Weinheim, 2008)
9. S. Schikora, H.-J. Wünsche, F. Henneberger, Phys. Rev. E **78**, 025202(R) (2008)
10. V.Z. Tronciu, H.-J. Wünsche, M. Wolfrum, M. Radziunas, Phys. Rev. E **73**, 046205 (2006)
11. S. Yanchuk, M. Wolfrum, P. Hövel, E. Schöll, Phys. Rev. E **74**, 026201 (2006)
12. V. Flunkert, E. Schöll, Phys. Rev. E **76**, 066202 (2007)

13. T. Dahms, P. Hövel, E. Schöll, Phys. Rev. E **76**, 056201 (2007)
14. T. Dahms, P. Hövel, E. Schöll, Phys. Rev. E **78**, 056213 (2008)
15. B. Fiedler, V. Flunkert, M. Georgi, P. Hövel, E. Schöll, Phys. Rev. Lett. **98**, 114101 (2007)
16. B. Fiedler, S. Yanchuk, V. Flunkert, P. Hövel, H.-J. Wünsche, E. Schöll, Phys. Rev. E **77**, 066207 (2008)
17. S. Schikora, Thesis (in preparation)
18. B. Fiedler, V. Flunkert, P. Hövel, E. Schöll, Eur. Phys. J. Special Topics **191**, 53 (2010)
19. K.-H. Lee, W.-Y. Choi, Y.A. Leem, K.H. Park, IEEE Phot. Technol. Lett. **19**, 161 (2007)
20. S. Schwertfeger, A. Klehr, A. Liero, G. Erbert, G. Tränkle, IEEE Phot. Technol. Lett. **19**, 1889 (2007)
21. A. Argyris, M. Hamacher, K.E. Chlouverakis, A. Bogris, D. Syvridis, Phys. Rev. Lett. **100**, 194101 (2008)
22. H.-J. Wünsche, S. Bauer, J. Kreissl, O. Ushakov, N. Korneyev, F. Henneberger, E. Wille, H. Erzgräber, M. Peil, W. Elsäßer, I. Fischer, Phys. Rev. Lett. **94**, 163901 (2005)
23. S. Bauer, O. Brox, J. Kreissl, B. Sartorius, M. Radziunas, J. Sieber, H.-J. Wünsche, F. Henneberger, Phys. Rev. E **69**, 016206 (2004)
24. U. Bandelow, H.-J. Wünsche, B. Sartorius, M. Möhrle, IEEE J. Sel. Top. Quantum Electron. **3**, 270 (1997)
25. M. Möhrle, B. Sartorius, C. Bornholdt, S. Bauer, O. Brox, A. Sigmund, R. Steingrüber, M. Radziunas, H.-J. Wünsche, IEEE Sel. Top. Quant. Electron. **7**, 217 (2001)
26. B. Dahmani, L. Hollberg, R. Drullinger, Opt. Lett. **12**, 876 (1987)
27. P. Laurent, A. Clairon, C. Breant, IEEE J. Quantum Electron. **25**, 1131 (1989)
28. M. Peil, I. Fischer, W. Elsäßer, Phys. Rev. A **73**, 23805 (2006)
29. H. Erzgräber, B. Krauskopf, D. Lenstra, A.P.A. Fischer, G. Vemuri, Phys. Rev. E **73**, 055201(R) (2006)
30. J.E.S. Socolar, D.W. Sukow, D.J. Gauthier, Phys. Rev. E **50**, 3245 (1994)
31. W. Just, D. Reckwerth, E. Reibold, H. Benner, Phys. Rev. E **59**, 2826 (1999)
32. P. Hövel, J.E.S. Socolar, Phys. Rev. E **68**, 036206 (2003)
33. Z. Gills, C. Iwata, R. Roy, I.B. Schwartz, I. Triandaf, Phys. Rev. Lett. **69**, 3169 (1992)
34. A. Ahlborn, U. Parlitz, Phys. Rev. Lett. **96**, 034102 (2006)
35. O. Ushakov, S. Bauer, O. Brox, H.-J. Wünsche, F. Henneberger, Phys. Rev. Lett. **92**, 043902 (2004)
36. R. Lang, K. Kobayashi, IEEE J. Quantum Electron. **16**, 347 (1980)
37. V.Z. Tronciu, H.-J. Wünsche, J. Sieber, K. Schneider, F. Henneberger, Opt. Commun. **182**, 221 (2000)
38. G.P. Agrawal, G.R. Gray, Phys. Rev. A **46**, 5890 (1992)
39. C. Simmendinger, O. Hess, Phys. Lett. A **216**, 97 (1996)
40. P.M. Alsing, V. Kovanis, A. Gavrielides, T. Erneux, Phys. Rev. A **53**, 4429 (1996)
41. Feature Section on Optical Chaos and Applications to Cryptography, IEEE J. Quant. Electron. **38**, 1138 (2002)
42. A. Argyris, D. Kanakidis, A. Bogris, D. Syvridis, IEEE J. Quant. Electron. **41**, 892 (2005)
43. T. Pérez, M. Radziunas, H.-J. Wünsche, C.R. Mirasso, F. Henneberger, IEEE Photon. Techn. Lett. **18**, 2135 (2006)
44. K. Petermann, *Laser Diode Modulation and Noise* (Kluwer Academic, Boston, 1991)
45. J.L.A. Dubbeldam, B. Krauskopf, D. Lenstra, Phys. Rev. E **60**, 6580 (1999)
46. G. Giacomelli, M. Giudici, S. Balle, J.R. Tredicce, Phys. Rev. Lett. **84**, 3298 (2000)
47. V.V. Sherstnev, A. Krier, A.G. Balanov, N.B. Janson, A.N. Silchenko, P.V.E. McClintock, Fluct. Noise Lett. **3**, 91 (2003)
48. O.V. Ushakov, H.J. Wünsche, F. Henneberger, I.A. Khovanov, L. Schimansky-Geier, M.A. Zaks, Phys. Rev. Lett. **95**, 123903 (2005)
49. V. Beato, I. Sendiña-Nadal, I. Gerdes, H. Engel, Phys. Rev. E **71**, 035204 (2005)
50. G. Stegemann, A.G. Balanov, E. Schöll, Phys. Rev. E **71**, 016221 (2005)
51. J. Hizanidis, A.G. Balanov, A. Amann, E. Schöll, Phys. Rev. Lett. **96**, 244104 (2006)

52. B. Lindner, J. García-Ojalvo, A. Neiman, L. Schimansky-Geier, Phys. Rep. **392**, 321 (2004)
53. N.B. Janson, A.G. Balanov, E. Schöll, Phys. Rev. Lett. **93**, 010601 (2004)
54. A.G. Balanov, N.B. Janson, E. Schöll, Physica D **199**, 1 (2004)
55. E. Schöll, A.G. Balanov, N.B. Janson, A. Neiman, Stoch. Dyn. **5**, 281 (2005)
56. J. Pomplun, A. Amann, E. Schöll, Europhys. Lett. **71**, 366 (2005)
57. J. Pomplun, A.G. Balanov, E. Schöll, Phys. Rev. E **75**, 040101(R) (2007)
58. T. Prager, H.P. Lerch, L. Schimansky-Geier, E. Schöll, J. Phys. A **40**, 11045 (2007)
59. R. Aust, P. Hövel, J. Hizanidis, E. Schöll, Eur. Phys. J. ST **187**, 77 (2010)
60. G. Stegemann, A.G. Balanov, E. Schöll, Phys. Rev. E **73**, 016203 (2006)
61. A.G. Balanov, V. Beato, N.B. Janson, H. Engel, E. Schöll, Phys. Rev. E **74**, 016214 (2006)
62. J. Hizanidis, E. Schöll, Phys. Rev. E **78**, 066205 (2008)
63. B. Hauschildt, N.B. Janson, A.G. Balanov, E. Schöll, Phys. Rev. E **74**, 051906 (2006)
64. S.A. Brandstetter, M.A. Dahlem, E. Schöll, Phil. Trans. R. Soc. A **368**, 391 (2010)
65. P. Hövel, S.A. Shah, M.A. Dahlem, E. Schöll, in *From Physics to Control through an Emergent View*, vol. 15 of *Nonlinear Science Seris B*, edited by L. Fortuna, A.L. Fradkov, M. Frasca (World Scientific, Singapore, 2010), p. 35
66. G.P. Agrawal, N.K. Dutta, *Semiconductor Lasers* (Van Nostrand Reinhold, New York, 1993)